

Wireless Energy Transmission Channel Modeling in Resonant Beam Charging for IoT Devices

Wei Wang[†], Qingqing Zhang[†], Hua Lin, Mingqing Liu, Xiaoyan Liang*, and Qingwen Liu*

Abstract—Power supply for Internet of Things (IoT) devices is one of the bottlenecks in IoT development. To provide perpetual power supply to IoT devices, resonant beam charging (RBC) is a promising safe, long-range and high-power wireless power transfer solution. How long distance can RBC reach and how much power can RBC transfer? In this paper, we analyze the RBC's consistent and steady operational conditions, which determine the maximum power transmission distance. Moreover, we study the power transmission efficiency within the operational distance, which determines the deliverable power through the RBC energy transmission channel. Based on this energy transmission channel modeling, we numerically evaluate its impacts on the RBC system performance in terms of the transmission distance, the transmission efficiency, and the output electrical power. The analysis leads to the guidelines for the RBC system design and implementation, which can deliver multi-Watt power over multi-meter distance wirelessly for IoT devices.

Index Terms—Resonant Beam Charging, Energy Transmission Channel Modeling, Wireless Power Transfer.

I. INTRODUCTION

With the development of the Internet of Things (IoT) [1–3] and the Big Data [4], the power supply for IoT devices has become one of the bottlenecks of IoT development. However, carrying power cord and looking for power supply cause inconvenience for people. The contradiction between battery endurance of IoT devices and the power supply is increasingly prominent [5–8]. Therefore, wireless power transfer (WPT) draws much attention to provide mobile power supply anywhere and anytime for IoT devices.

Several kinds of WPT technologies have been well investigated in research [9, 10]. Inductive coupling [11] is safe and simple but limited by a short charging distance from a few millimeters to centimeters. Magnetic resonance coupling [12, 13] has high charging efficiency, however it is restricted by a short charging distance and a large coil size. Radio frequency (RF) [14] has a long effective charging distance. However, it suffers low efficiency and difficulty to balance safety and high power. Laser charging [15, 16] needs directional pointing and can transmit high power to a long distance. But it also faces the radiation safety challenge. In summary, these technologies face with technical challenges to satisfy safety, long-range, high-power at the same time.

W. Wang, H. Lin and X. Liang, are with the State Key Laboratory of High Field Laser Physics, Shanghai Institute of Optics and Fine Mechanics, Chinese Academy of Sciences, Shanghai, China. W. Wang is also with the University of Chinese Academy of Sciences, Beijing 100049, China, (email: wangwei2016@siom.ac.cn, hual@siom.ac.cn, liangxy@siom.ac.cn).

Q. Zhang, M. Liu, and Q. Liu, are with the College of Electronic and Information Engineering, Tongji University, Shanghai, China, (email: anne@tongji.edu.cn, 18392105294@163.com, qliu@tongji.edu.cn).

[†] Both authors contributed equally to this work.

* Corresponding author.

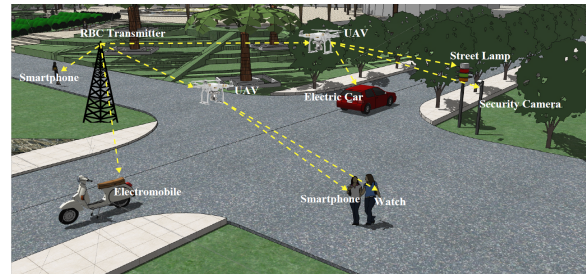


Fig. 1 Resonant Beam Charging Application

Resonant beam charging (RBC), as known as distributed laser charging (DLC), is presented in [17] which can safely provide multi-Watt wireless power supply over multi-meter distance for IoT devices. In the RBC system, any object blocking the line of sight (LOS) between the transmitter and the receiver can break resonance immediately, which leads to the inherent safety. Meanwhile when the RBC system operates as a stable resonant cavity, even slight blocking of the beam will instantly cause a significant alteration in the beam's power, which makes it simple to detect such a blocking. Furthermore, any bystander outside of the resonant cavity limits will not be subjected to any of the beam's radiation. The adaptive resonant beam charging (ARBC) system proposed in [18] improved the WPT efficiency based on feedback control. Moreover, the RBC not only can achieve self-aligning, but also can charge multi-devices simultaneously.

Fig. 1 illustrates the RBC potential application. As shown in Fig. 1, the RBC transmitter can be mounted on a communication base station, which can provide wireless power to electromobile and mobile devices within its coverage. In addition, the unmanned aerial vehicle (UAV) equipped with both the RBC transmitter and receiver can play the role of a relay to receive power from the RBC transmitter and transmit power to IoT devices within its coverage. The RBC is a promising solution to break the power supply bottleneck in development of IoT. However, how long distance RBC can reach and how much power RBC can transfer are essential issues to investigate. The contributions of this paper include: 1) We present the analytical model of the energy transmission channel for the RBC system and study the RBC's consistent and steady operational conditions and the power transmission efficiency within the operational distance; 2) We numerically evaluate its impacts on the RBC system performance in terms of the transmission distance, the transmission efficiency, and the output electrical power; 3) We derive the closed-formula for the relationship among the end-to-end power, efficiency and transmission distance, which provide guidelines for the

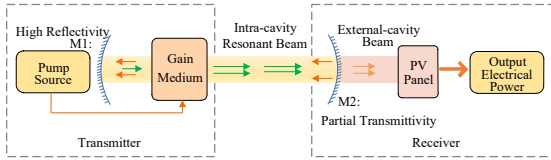


Fig. 2 Resonant Beam Charging System

RBC system design and implementation.

In the rest of this paper, we will briefly introduce the RBC system at first. Then, we will give the modular model and working mechanism of the RBC system. Based on the analytical analysis, we will depict the system performance in the next section. Finally, we will make a conclusion and discuss open issues for future research.

II. RESONANT BEAM CHARGING

The resonant beam charging (RBC) is a WPT technology which transfers power through intra-cavity resonant beam. In the RBC system, the optical components are divided into two separate parts: the transmitter and the receiver. The architecture of the RBC system is shown in Fig. 2. In the RBC transmitter, there is a high reflectivity curved mirror M1 and a gain medium pumped by pump source. The pump source excites gain medium to realize population inversion, which leads to energy storage in the gain medium. The energy stored in the gain medium is determined by the input electrical power, the performance of pump source, the pump chamber structure, and the property of gain medium [19].

While in the RBC receiver, a partial transmittivity curved mirror M2 is contained. M1 and M2 constitute the optical resonant cavity, which performs the function of a highly selective feedback element by coupling a portion of the signal generated from the gain medium in phase. The resonant cavity should satisfy steady condition for providing sufficient large feedback for the RBC system. At the same time, satisfy steady condition can ensure high safety and efficiency for the resonant cavity. If the feedback is large enough to compensate the internal losses of the system, the system starts to oscillate. When the system is triggered by the spontaneous radiation emitted along the axis of the resonant cavity. Thus, the gain medium stored energy is released to the intra-cavity resonant beam by stimulated emission [19]. The transmission efficiency relies on the energy transmission distance of the system and the loss related to the transverse mode.

The beam emitted by most optical resonant cavity contains several discrete optical frequencies. The beams are separated from each other due to frequency differences which can lead to different modes of the optical resonant cavity. Each mode is defined by the variation of the electromagnetic field perpendicular and along the axis of the resonant cavity. It is common to distinguish two types of resonant cavity modes: longitudinal modes which differ from each other only in their oscillation frequency; transverse modes which differ from each other not only in their oscillation frequency, but also in their field distribution in a plane perpendicular to the direction of propagation [19].

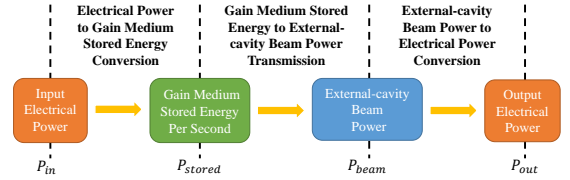


Fig. 3 Modular Model of the RBC System

The loss affects the gain medium stored energy to intra-cavity beam power transmission efficiency. There are two kinds of loss with different properties in the RBC system [20]. The first kind is the loss independent of the resonant beam transverse mode, such as the internal loss of the gain medium, the transmission loss of the mirror, the absorption, and scattering loss of the element in the system. The other is the diffraction loss that closely related to the transverse mode and the transmission distance.

At the same time in the RBC receiver, a photovoltaic panel (PV-panel) is installed behind the mirror M2. The power of intra-cavity resonant beam is extracted from the partial transmittivity mirror M2. The external-cavity beam power can be converted to electrical power by the PV-panel. The beam power-to-electrical power conversion is based on the PV engineering [21–23].

III. ANALYTICAL MODELING FOR ENERGY TRANSMISSION

In the RBC system, the input electrical power will be converted to the gain medium stored energy. Then, the gain medium stored energy will be converted to the intra-cavity resonant beam power, which will be transmitted from the transmitter to the receiver over a certain distance. Then, the intra-cavity resonant beam power will be partially converted to the external-cavity beam power at the receiver. Finally, the external-cavity beam power will be converted to the output electrical power, which can be used to charge devices accessed to the RBC system.

In this section, we will illustrate the analytical modeling of the RBC energy transmission channel by dividing the procedure into three stages: the input electrical power to the gain medium stored energy conversion, the gain medium stored energy to the external-cavity beam power transmission, and the external-cavity beam power to the output electrical power conversion. Fig. 3 gives the modular model and the three energy transmission stages of the RBC system.

A. Electrical Power-to-Stored Energy Conversion

The input electrical power P_{in} , which is provided by the driving source, acts on the pump source. The pump source transforms the electrical power into the pump power which can be absorbed by the gain medium. Then, the pump power is transferred to the gain medium through a completely enclosed reflective chamber i.e. pump chamber. The absorbed pump power excites the gain medium to realize the population inversion, and then the energy is stored in the gain medium.

In the case of continuous input of electrical power, the relationship between the gain medium stored energy per second P_{stored} and the input electrical power P_{in} can be depicted as [19]:

$$P_{stored} = \eta_{stored} P_{in}, \quad (1)$$

where η_{stored} is the electrical power-to-stored energy conversion efficiency. It is affected by the performance of the pump source, the pump chamber structure, and the material and size of gain medium [19]. η_{stored} can be computed as:

$$\eta_{stored} = \frac{P_{stored}}{P_{in}}. \quad (2)$$

Most of the input electrical power which can not be converted to the stored energy is dissipated as heat.

B. Stored Energy-to-Beam Power Transmission

The stored energy at the transmitter can be triggered by the spontaneous radiation emitted along the axis of the resonant cavity, and be converted to the intra-cavity resonant beam power. After part of the intra-cavity resonant beam passing through the partial transmittivity mirror M2, the external-cavity beam is formed. Therefore, with the transmission attenuation in the free space, the stored energy will be converted into the external-cavity beam power. Since both the transmission distance and the transmission efficiency have effects on the stored energy to beam power transmission efficiency, we will give the transmission distance model at first. Then, we will analyze the factors which influence the transmission efficiency.

1) *Transmission Distance Modeling*: To support the energy transmission, the resonant cavity should keep stable at first. Factors that influence the stable condition include the material and construction of the gain medium, the curvature radius of the mirror at the transmitter M1 and that of the mirror at the receiver M2, the distance between the gain medium and M1 l , and the distance between the gain medium and M2 d .

A resonant cavity containing a rod shaped gain medium is taken as an example. In the rod, the heat generation is uniform, which acts as a lens-like medium since, due to thermal and stress-induced effects. From [24], the resonant cavity can be represented by a model containing a thin lens, as shown in Fig. 4. Where the gain medium is replaced by a thin lens with a focal length of f , R_1 is the curvature radius of M1 mirror, R_2 is the curvature radius of M2 mirror, l represents the space size of the transmitter, d represents the transmission distance. We define the effective resonant cavity length L as:

$$L = l + d - \frac{ld}{f}. \quad (3)$$

To express the stability condition of the resonant cavity more clearly, we introducing g_1 , g_2 as:

$$g_1 = 1 - \frac{d}{f} - \frac{L}{R_1}, \quad (4)$$

$$g_2 = 1 - \frac{l}{f} - \frac{L}{R_2}. \quad (5)$$

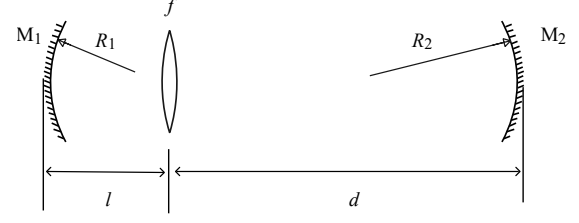


Fig. 4 Schematic Diagram of Resonant Cavity with Thermal Lens

As can be seen, g_1 and g_2 are both related to the transmission distance d . According to [25], to keep the RBC system working at the stability condition, the following condition should be satisfied:

$$0 < g_1 g_2 < 1. \quad (6)$$

To show graphically which type of resonant cavity is stable and which is unstable, it is useful to plot a stability diagram Fig. 5. In Fig. 5, each particular resonant cavity geometry is represented by a point to show the stable or unstable resonant cavity type. All cavity configurations are unstable unless they correspond to points located in the area enclosed by a branch of the hyperbola $g_1 g_2 = 1$ and the coordinate axes, as shown in the shadow part of Fig. 5. As the distance d varies, the straight line in Fig. 5 is derived by eliminating d in (4) and (5):

$$g_2 = \frac{(l-f)R_1}{(l-R_1-f)R_2} g_1 + \frac{(l-f)(l-R_1)}{(l-R_1-f)R_2} + 1 - \frac{l}{f} - \frac{l}{R_2}. \quad (7)$$

The two straight lines in Fig. 5 correspond to two general situations. The intersections of the straight line with the axes and with the hyperbola $g_1 g_2 = 1$ gives the critical values of d corresponding to the edges of the stability regions [26]. In our theoretical model, the range of d satisfying the stability condition represents the distance range that can realize energy transmission. The critical value of d determines the maximum transmission distance of the RBC system.

Though the intensity distribution on each section of the resonant beam is consistent, the beam radius (defined as the radius at which the electric field amplitude is down by $1/e$ from the maximum) of the intensity distribution varies along the optical axis [19]. For analyzing the relationship between the beam radius of each location and the transmission distance more concisely, we introduce three new variables u_1 , u_2 , and x as:

$$u_1 = l \left(1 - \frac{l}{R_1} \right), \quad (8)$$

$$u_2 = d \left(1 - \frac{d}{R_2} \right), \quad (9)$$

$$x = \frac{1}{f} - \frac{1}{l} - \frac{1}{d}. \quad (10)$$

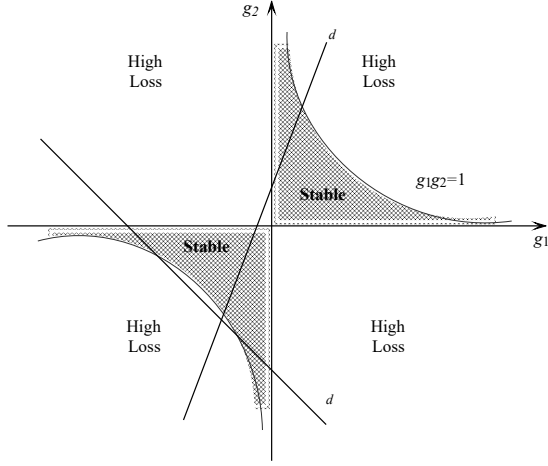


Fig. 5 Stability Diagrams

The beam radius on gain medium ω_1 , on M1 ω_2 and on M2 ω_3 can be expressed as [26]:

$$\omega_1 = \sqrt{\frac{\lambda}{\pi} \frac{|2xu_1u_2 + u_1 + u_2|}{[(1 - g_1g_2)g_1g_2]^{1/2}}}, \quad (11)$$

$$\omega_2 = \sqrt{\frac{\lambda|L|}{\pi} \left[\frac{g_2}{g_1(1 - g_1g_2)} \right]^{1/2}}, \quad (12)$$

$$\omega_3 = \sqrt{\frac{\lambda|L|}{\pi} \left[\frac{g_1}{g_2(1 - g_1g_2)} \right]^{1/2}}. \quad (13)$$

However, due to losses of the RBC system, the maximum transmission distance can not be actually obtained. There are two kinds of loss influencing the transmission: the loss independent of the beam transverse mode, and the diffraction loss closely related to the transverse mode [20]. The loss independent of transmission mode is determined by the intrinsic nature of the components used by the system. Therefore, we only take the transverse mode related diffraction loss into consideration.

2) *Transmission Efficiency Modeling*: The diffraction loss is mainly caused by the diffraction effect. According to [27], resonant beam is a beam oscillation with the feedback of the resonant cavity and the gain medium. When the resonant beam travels back and forth between the M1 and M2, the edge of the mirror M1 and M2 will cause loss due to the diffraction effect. Because the mirror geometry of M1 and M2 is limited, as shown in Fig. 6, where a presents the radius of the end mirror M1 and M2 of the optical resonant cavity. As shown in the Fig. 6, after a number of round-trip propagation, the electric field distributions of the cross section of a resonant beam on the mirror M1 and M2 are $E_1(x, y)$, and $E_2(x, y)$. Then, there should be the following self consistent relationship [27]:

$$E_2(x, y) = \gamma E_1(x, y), \quad (14)$$

where γ is a complex constant factor, which reflects the change of amplitude and phase of beam field after a one-

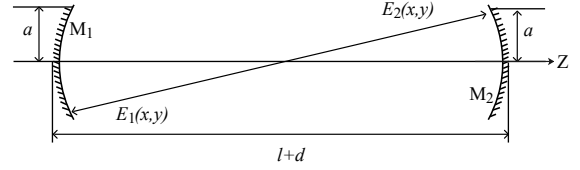


Fig. 6 Schematic Diagram of Stable Resonant Cavity

way propagation. The total energy loss of single trip δ can be expressed as:

$$\delta = \frac{|E_1|^2 - |E_2|^2}{|E_1|^2} = 1 - |\gamma|^2. \quad (15)$$

The loss which independent of the beam transverse mode, such as transmission, absorption and output, is depending on the intrinsic properties of the components. Therefore this loss is not considered in our model. Thus γ only contains the diffraction loss of the edge of the mirror M1 and M2. Meanwhile, the diffraction loss is caused not only by the optical resonant cavity end mirrors, but also by finite aperture in the resonant cavity, such as the aperture of gain medium. According to [28], the diffraction loss of the beam through a aperture with an diameter of $2a$ in the optical resonant cavity δ_{mn} is:

$$\delta_{mn} = 1 - \frac{\int_0^{2\pi} \int_0^a r^{2m} \left[L_n^m \left(\frac{2r^2}{\omega^2} \right) \right]^2 e^{-2\frac{r^2}{\omega^2}} r dr d\varphi}{\int_0^{2\pi} \int_0^\infty r^{2m} \left[L_n^m \left(\frac{2r^2}{\omega^2} \right) \right]^2 e^{-2\frac{r^2}{\omega^2}} r dr d\varphi}, \quad (16)$$

where m, n are positive integers, r is the radial radius, φ is phase difference, and $L_n^m(\xi)$ is n order associative Laguerre polynomials.

For the general stable optical resonant cavity, the equivalent principle of the confocal resonator can be used to transform the diffraction loss [27]. In the RBC system, to improve the uniformity of beam cross section energy distribution, the resonant beam is the superposition of TEM_{00} mode and multiple higher order modes. The TEM_{00} presents the fundamental mode in a optical resonant cavity, which is inevitable in resonant cavity. Furthermore, the high-order mode is with large number, and being difficult to be analyzed. Since the diffraction loss of the higher order mode is proportional to the TEM_{00} mode, we only take the diffraction loss of TEM_{00} mode into consideration in this paper. The diffraction loss $\delta_{00}(d)$ of TEM_{00} mode, which is related with d , can be presented as:

$$\delta_{00}(d) = e^{-2\pi \frac{a^2}{\lambda(i+d)}}. \quad (17)$$

To sum up, given the gain medium and certain structure of the resonant cavity, the external-cavity beam power P_{beam} can be stimulated by the stored power P_{stored} . The relationship between P_{beam} and P_{stored} can be depicted as [19]:

$$P_{beam} = f(d)P_{stored} + C, \quad (18)$$

where $f(d)$ is the equation related to the transmission distance d , and C is a constant which depends on the internal parameters of the system.

With reference to (17) and [19], $f(d)$, which is closely related with the diffraction loss δ_{00} , can be computed as:

$$\begin{aligned} f(d) &= \frac{2(1-R)m}{(1+R)\delta_{00}(d) - (1+R)\ln R} \\ &= \frac{2(1-R)m}{(1+R)e^{-2\pi\frac{a^2}{\lambda(l+d)}} - (1+R)\ln R}, \end{aligned} \quad (19)$$

where R is the reflectivity of the output mirror M2, and m is the overlap efficiency.

Therefore, we can obtain the stored energy to beam power transmission efficiency η_{trans} :

$$\eta_{trans} = \frac{P_{beam}}{P_{stored}} = f(d) + \frac{C}{P_{stored}}. \quad (20)$$

C. Beam Power-to-Electrical Power Conversion

At the RBC receiver, the external-cavity beam power can be converted to electrical power, which can be used to charge devices accessed to the RBC system. For certain input beam power, the output electrical power will be different if with different load in the circuit. To obtain the maximum beam power to electrical power conversion efficiency, the PV-panel should work at the maximum output power state with the assistance of maximum power point tracking (MPPT) technology. As stated in [18], the maximum PV-panel output power P_{pv} takes a linear relationship with the external-cavity beam power P_{beam} , which is as:

$$P_{pv} = a_1 P_{beam} + b_1. \quad (21)$$

Therefore, the beam power-to-electrical power conversion efficiency, i.e. the PV-panel conversion efficiency, η_{pv} depends on P_{pv} and P_{beam} , which can be depicted as:

$$\eta_{pv} = \frac{P_{pv}}{P_{beam}} = a_1 + \frac{b_1}{P_{beam}}. \quad (22)$$

In summary, the PV-panel converts the received beam power P_{beam} to the output electrical power P_{pv} with the conversion efficiency η_{pv} .

D. End-to-end Power Transmission

Based on the above theoretical analysis for each procedure, the end-to-end power relationship, that is the relationship between the input electrical power and the output electrical power, can be depicted as:

$$\begin{aligned} P_{out} &= a_1[f(d)P_{stored} + C] + b_1 \\ &= a_1f(d)\eta_{stored}P_{in} + a_1C + b_1. \end{aligned} \quad (23)$$

As can be seen, the system output power P_{out} is affected by the input power P_{in} and the transmission distance d at the same time. Based on (23), the relationship between the end-to-end transmission efficiency η_{all} and the input electrical power can be obtained as:

$$\begin{aligned} \eta_{all} &= \eta_{stored}\eta_{trans}\eta_{pv} \\ &= a_1\eta_{stored}\eta_{trans} + \frac{b_1}{P_{in}} \\ &= a_1\eta_{stored}f(d) + \frac{a_1C + b_1}{P_{in}}. \end{aligned} \quad (24)$$

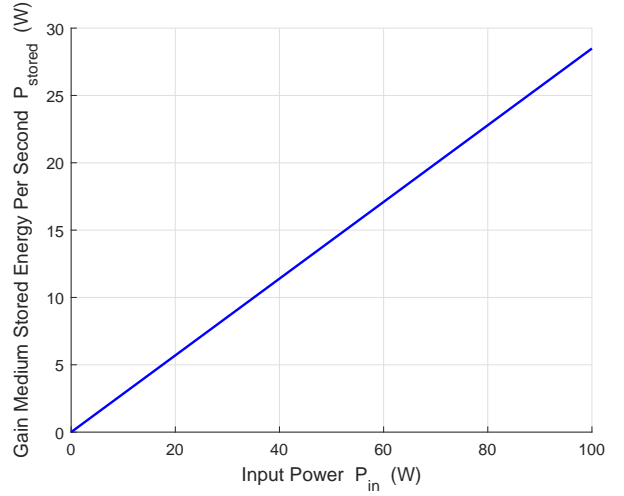


Fig. 7 Gain Medium Stored Energy Per Second vs. Input Power

As can be seen, η_{all} is affected by both P_{in} and d .

The transmission or conversion efficiency of each module and the RBC power transmission efficiency are listed in Table I.

The analytical modeling of the RBC energy transmission is illustrated, and the factors influencing the energy transmission are analyzed in this section. On this basis, the performance evaluation of the RBC system will be presented in the next section.

IV. PERFORMANCE EVALUATION

Based on the analytical modeling in the previous section, we can find that the RBC system efficiency varies with the input electrical power, the electrical power to stored energy conversion efficiency, the material and size of the gain medium, the transmission distance, the reflectivity of the mirrors, the overlap efficiency, the diffraction loss of the intra-cavity beam, and the beam power to the electrical power conversion efficiency. In this section, we will give the numerical evaluation of the RBC system in certain scenarios. All the numerical evaluations are implemented in MATLAB and Simulink.

A. Electrical Power-to-Stored Energy Conversion

At the RBC transmitter, the input electrical power P_{in} is converted to the gain medium stored energy per second

TABLE I Transmission or Conversion Efficiency

Parameter	Description
η_{stored}	electrical power to gain medium stored energy conversion efficiency
η_{trans}	gain medium stored energy to external-cavity beam power transmission efficiency
η_{pv}	external-cavity beam power to electrical power conversion efficiency
η_{all}	end-to-end transmission efficiency

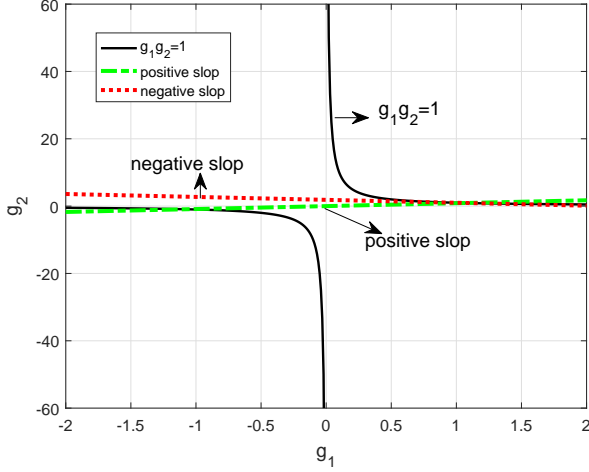


Fig. 8 Connected Stability Diagrams

P_{stored} . The conversion efficiency is determined by the performance of pump source, the structure of the pump chamber and the material and size of the gain medium. Here we use the 808nm laser diode as the pump source, and the Nd:YAG rod, which is side pumped by the laser diode, as the gain medium. For the rod, the length is 65mm, the diameter is 3mm, and the stimulated beam is of 1064nm. According to [19], the electrical power to stored energy conversion efficiency η_{stored} takes 28.49%.

Then, with reference to (1), the relationship between P_{stored} and P_{in} can be depicted out, as shown in Fig. 7. As can be seen, P_{stored} goes up linearly as P_{in} increases, and the straight line between P_{stored} and P_{in} passes through the origin.

B. Stored Energy-to-Beam Power Transmission

In this part, we will illustrate how to design the cavity structure and select the transmission distance, and how the transmission distance influences the stored energy to beam power transmission efficiency.

1) *Transmission Distance Modeling*: According to (3), (4), (5), and (7), given resonant cavity configuration, i.e. given l , f , R_1 , and R_2 , the position of a straight line in Fig. 5 is determined. Usually the focal length f for Nd materials ranges from a few meters to a few tens of centimeters [19]. We set up $f = 880mm$ according to the results of experimental measurements. According to the geometric parameters of the gain medium used in practice, the shortest l is 60mm. Usually we can obtain two distinct stability zones as shown in Fig. 5. In an ideal wireless power transmission device, it is not desirable to have a range of distances that power can not be transferred within the maximum distance allowed. Thus we expect the transmission range to be continuous, that is, the two stability regions are connected.

To connect the two stability regions, the position of a straight line in Fig. 5 needs satisfy the intersection point of the straight line and the coordinate axis is coincident or the intersection point of the straight line and the $g_1g_2 = 1$ curve is

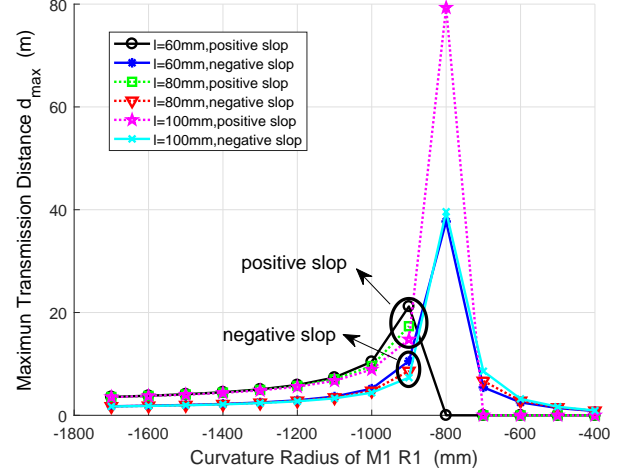


Fig. 9 Maximum Transmission Distance vs. Curvature Radius of M1

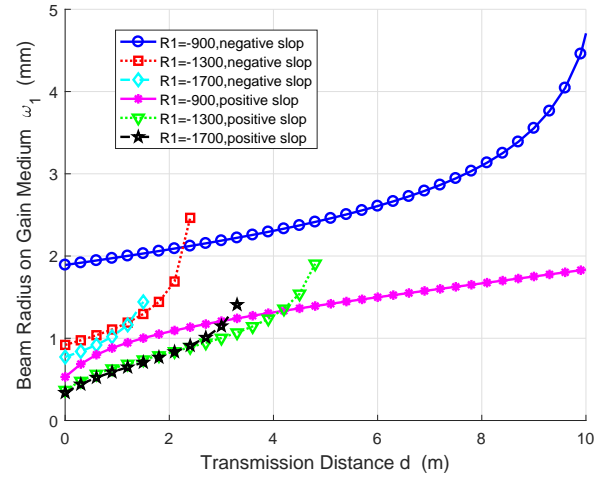


Fig. 10 Beam Radius on Gain Medium vs. Transmission Distance

coincident. There are two solutions: 1) the straight line slope is positive, and through the origin; 2) the straight line slope is negative, and tangent to $g_1g_2 = 1$. Fig. 8 shows the two situations that can connect two stability regions. The dashed presents the line of positive slope and the dotted line presents the line of negative slope. We can find that every set of values of R_1 and l has two R_2 solutions, which is corresponding to two cases in Fig. 8.

No matter which cases the system works at, given l and R_1 , the maximum intra-cavity resonant beam transmission distance d_{max} can be different. The relationships among l , R_1 and d_{max} in the two cases are given in Fig. 9. From Fig. 9, when $R_1 = -800mm$, the solution of the negative slope about maximum transmission distance reaches the maximum as about 40m. The maximum of positive slope is about 80m. When $R_1 < -900mm$, the solution of positive slope is larger than that of the negative slope about maximum transmission distance. When l takes 60mm, 80mm and 100mm, the maximum transmission distance is slightly different. In order

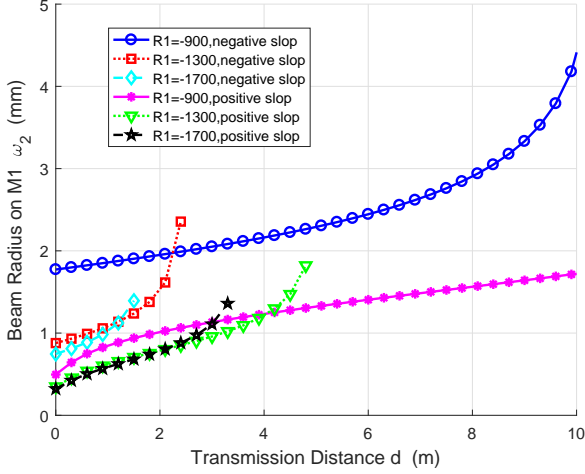


Fig. 11 Beam Radius on M1 vs. Transmission Distance

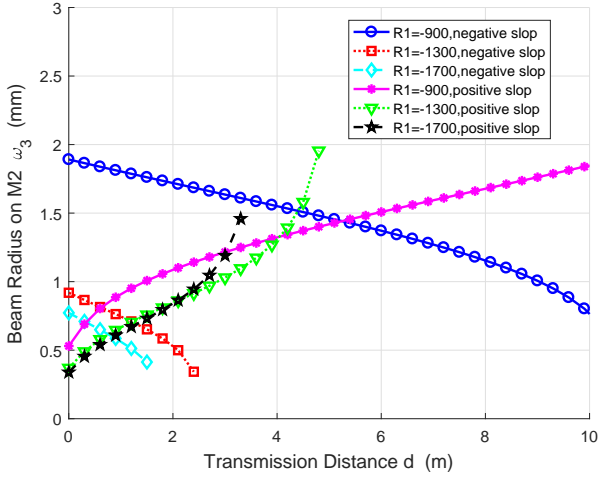


Fig. 12 Beam Radius on M2 vs. Transmission Distance

to make the volume of the transmitter as small as possible, we set up $l = 60\text{mm}$.

Therefore, the beam transmission distance d can take any value lower than d_{max} . However, with the variation of d , the beam radiuses on the gain medium ω_1 , on M1 ω_2 , and on M2 ω_3 take different value. Based on (4), (5), (11), (12), and (13), how ω_1 , ω_2 , ω_3 change as d varies are given in Fig. 10, Fig. 11 and Fig. 12, respectively.

As can be seen, in the case of positive slope, the beam radiuses on gain medium ω_1 , on M1 ω_2 and on M2 ω_3 increase with the increment of transmission distance. However, in the case of negative slope, the beam radiuses ω_1 , ω_2 increase with the increment of transmission distance, while the beam radius ω_3 is the opposite. At the same time, if with same $R1$, the beam radiuses ω_1 and ω_2 are smaller in the case of positive slope than that of negative slope.

The size of the beam radius on gain medium determines the minimum size of the gain medium, and the cost of the gain medium is determined by the size. In addition, the size of the gain medium will also affect the transmitter's size. For

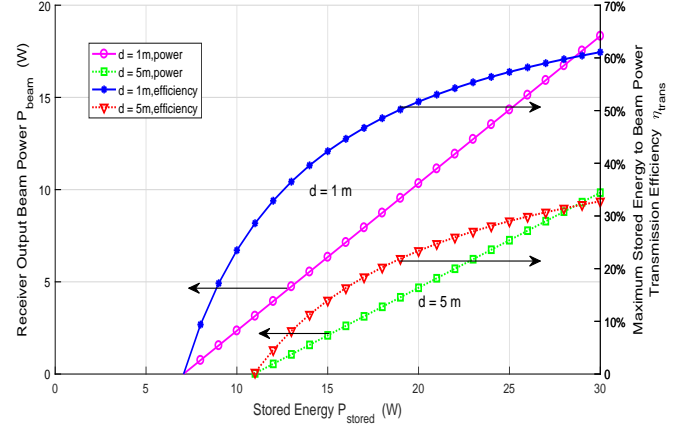


Fig. 13 Beam Power and Transmission Efficiency vs. Stored Energy

practical applications, the transmitter should be as smaller as possible. Given certain $R1$, to guarantee longer transmission distance and reduce the size of the transmitter and the cost of the gain medium, we chose the stability region with the positive slope.

For practical applications, we expect that the maximum transmission distance of the RBC system is at least $5m$. According to Fig. 9, the $R1$ should satisfy $-1300\text{mm} \leq R1 \leq -900\text{mm}$ in the case of positive slope.

2) *Transmission Efficiency Modeling*: After the above analysis, the transmission distance and the structure of the resonant cavity are determined. As in [19], R of the mirror M2 in the receiver is 0.88, the overlap efficiency m is 1 and C can be -5.64 . From (18) and (19), given d , the function $f(d)$ becomes a constant, so P_{beam} linearly depends on P_{stored} . To explore the relationship between P_{beam} and P_{stored} , we set d with $1m$ and $5m$. The relationships are shown as the linear lines in Fig. 13. As can be seen, when P_{stored} is over the threshold, P_{beam} increases as P_{stored} increases. On the other hand, the threshold goes up if d is larger. This is because that more stored energy attenuates when passing over a longer distance. Therefore, for certain P_{stored} , P_{beam} takes smaller value when d takes bigger value.

For the same d , the stored energy to the beam power conversion efficiency η_{trans} can be obtained according to (20). The relationship between η_{trans} and P_{stored} are given as the non-linear curves in Fig. 13. After P_{stored} is over the threshold, η_{trans} goes up dramatically at first, and then its growing trend becomes slow. At the same time, η_{trans} takes smaller value if the beam goes through a longer distance. If the transmitting distance is $1m$, η_{trans} can be up to about 61% when P_{stored} is $30W$.

From (18), if P_{stored} is given, with reference to (20), the function $f(d)$ varies with the transmitting distance d , and P_{beam} relies on d . Curves in Fig. 14 depicts how P_{beam} and η_{trans} changes with d , when P_{beam} takes $10W$, $20W$, and $30W$, respectively. When the d takes small values at first, P_{beam} keeps almost steady. Then, as d goes up, P_{beam} goes down. Compared with the downward trend of P_{beam} with low

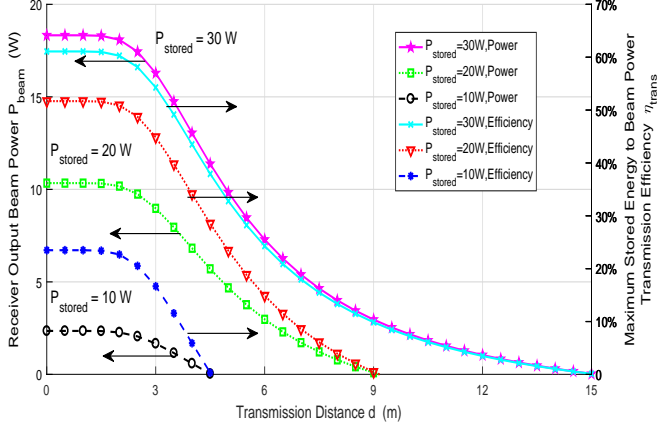


Fig. 14 Beam Power and Transmission Efficiency vs. Transmission Distance

value, the downward trend of P_{beam} with high value is much slower. Meanwhile, if with same d , higher P_{stored} guarantees higher P_{beam} being received at the receiver.

While, the changing trend of η_{trans} over d is similar with that of P_{beam} when P_{stored} takes same value. At the same time, for same d , η_{trans} takes higher values when P_{stored} takes higher value. For example, if d is $3m$, η_{trans} is more than 50% when $P_{stored} = 30W$, while η_{trans} is about 40% when $P_{stored} = 20W$, and η_{trans} only takes lower than 20% when $P_{stored} = 10W$. In the gain medium stored energy, part of the energy that is not converted to resonant beam is scattered into the surrounding environment. Safety can be guaranteed because the scattered power is with a very low power density.

C. Beam Power-to-Electrical Power Conversion

At the RBC receiver, the PV-panel takes the role of converting the external-cavity beam power to the electrical power. Here we use the $808nm$ laser diode side pumped $1064nm$ Nd:YAG rod to establish the RBC system with $2m$ transmission distance, and record all the measured data. After analyzing the data with Simulink, we can obtain the value of a_1 and b_1 in (21), which are 0.3487 and -1.535 respectively.

Therefore, we can obtain the relationship between the maximum PV-panel output power P_{pv} and the received external-cavity beam power P_{beam} , which is shown as the linear line in Fig. 15. As only after accumulating a certain amount of energy can the PV-panel converts the external-cavity beam power to the electrical power, there is a threshold before the electrical power is output. After P_{beam} becomes larger than the threshold, P_{pv} increases over P_{beam} .

Then, the relationship between the PV-panel efficiency η_{pv} and P_{beam} can be obtained. The non-linear curve in Fig. 15 presents the relationship. After P_{beam} is larger than the threshold, η_{pv} goes up dramatically as P_{beam} increases. Then η_{pv} increases more slowly, and the maximum value of η_{pv} is about 27%.

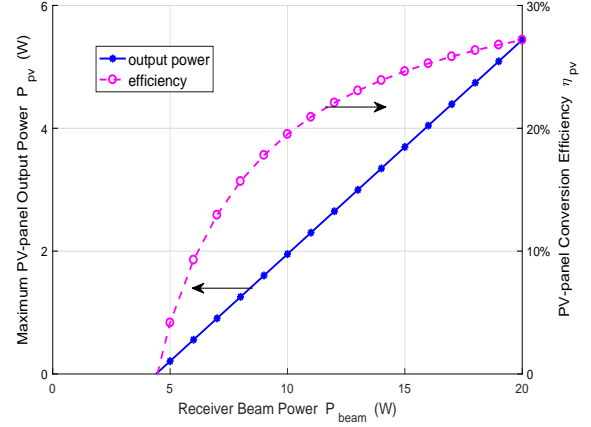


Fig. 15 PV-panel Output Power and Conversion Efficiency vs. Beam Power

D. End-to-end Power Transmission

Based on the above analysis, the end-to-end power transmission procedure, that is the whole RBC charging system energy transmission procedure, can be depicted. The end-to-end power relationship, that is the relationship between the input electrical power for driving the system and the output electrical power for charging devices, can be obtained. Based on (23), when the transmission distance d is given, the end-to-end power takes a linear relationship, which can be depicted as the linear lines in Fig. 16. As stated above, there are thresholds of the stored energy to the beam power transmission and the beam power to the electrical power conversion, and there is a threshold in the end-to-end power conversion relationship. After exceeding the threshold, P_{out} goes up linearly as P_{in} increases. At the same time, if with same P_{in} , the shorter distance guarantees the bigger P_{out} .

Then, from (24), how the end-to-end power transmission efficiency η_{all} changes over P_{in} can be obtained. The non-linear curves in Fig. 16 depict the relationship between η_{all} and P_{in} . As can be seen, η_{all} goes up gradually with the increment of P_{in} after that P_{in} is over the threshold. From Fig. 16, we can obtain how much input power should be provided if we want to charge devices with certain power at certain distance. For example, if we want to charge our devices with $1W$, when the distance from our devices to the RBC transmitter is $1m$, the input power to the transmitter should be about $55W$; while if the distance is $5m$, the input power should be about $85W$. At the same time, the corresponding end-to-end efficiency can be obtained under each condition as well.

On the other hand, for certain P_{in} , the changing trend among P_{out} , η_{all} and the transmission distance d can be depicted. Fig. 17 gives all the relationships when P_{in} takes $50W$, $80W$, and $100W$. P_{out} keeps almost steady when d is relatively short. Then, with the increment of d , P_{out} goes down dramatically. For different P_{in} , the declination takes different magnitude. The magnitude of the declines in P_{out} when P_{in} takes $100W$ is slower than that when P_{in} takes $80W$, which is slower than that when P_{in} takes $50W$.

The changing law of η_{all} over d has similar trend with

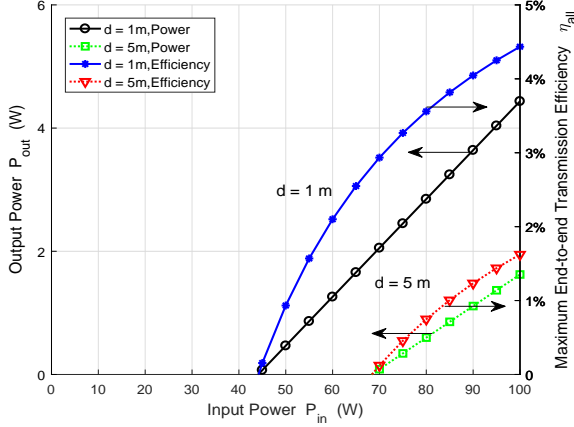


Fig. 16 Output Power and Transmission Efficiency vs. Input Power

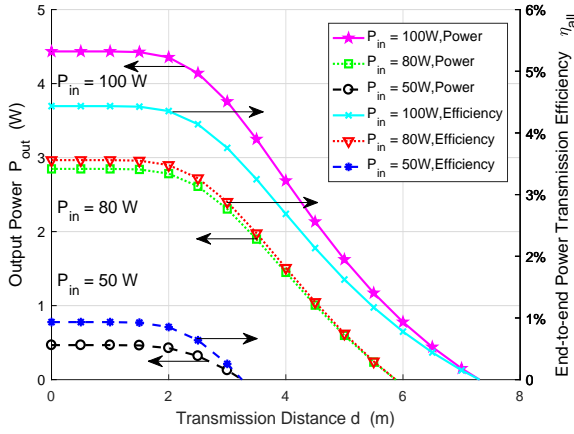


Fig. 17 Output Power and Transmission Efficiency vs. Transmission Distance

that of P_{out} when P_{in} takes same value. η_{all} keeps almost steady at first and then decreases dramatically as well. Meanwhile, the RBC charging system is more efficient when P_{in} takes larger value. When $P_{in} = 100W$, the maximum η_{all} is about 4.5%.

Fig. 17 provides guidelines for power control, efficiency control and distance selection when designing the RBC system. For example, if we want to support charging devices within $2m$, and design a system with about 4% efficiency, we should provide $100W$ input power or about $3.6W$ output power. If we want to charge devices with $1.5W$ power, and the transmission distance should be as long as $4m$, then the preferred input power should be $80W$, and the end-to-end efficiency is about 3%. In summary, the factors influencing the overall RBC efficiency include the input electrical power, the electrical power to stored energy conversion efficiency, the transmission distance and the PV-panel conversion efficiency. While the maximum transmission distance is decided by the stability conditions of the optical resonant cavity, the material and size of the gain medium, the diameter of the transmitter and the receiver, and the diffraction loss. We can obtain the following information from the above analysis:

- We obtain the maximum energy transmission distance d for the RBC system.
- We analyze the factors that influence the energy transmission power and efficiency, and gives their attenuation model over d .
- We derive the end-to-end RBC energy transmission efficiency η_{all} in closed-form.
- We analyze the relationships among P_{out} , η_{all} , P_{in} , and d under different circumstances, which lead to the design and development guidelines for the RBC system.

V. CONCLUSIONS

To provide perpetual power supply to IoT devices, resonant beam charging (RBC) is a promising safe, long-range and high-power wireless power transfer solution. In this paper, we present the analytical model of the energy transmission channel for the resonant beam charging (RBC) system, and study how long distance RBC can reach and how much power RBC can transfer. Based on the energy transmission channel modeling, we illustrate the RBC system performance influenced by the transmission distance, the transmission efficiency, and the output electrical power. These analysis lead to the guidelines for the RBC system design and implementation, which can deliver multi-Watt power over multi-meter distance wirelessly for IoT devices.

There are some open issues to be studied in future work.

For example:

- Since there are other loss factors influencing the RBC efficiency in addition to the diffraction loss. How to improve the overall efficiency of the RBC system should be further investigated.
- The RBC system performance will also be affected by other factors such as temperature. Thus the stability and reliability of the RBC system need further study.

REFERENCES

- [1] Y. Zhou, C. Huang, T. Jiang, and S. Cui, "Wireless sensor networks and the internet of things: Optimal estimation with nonuniform quantization and bandwidth allocation," *IEEE Sensors Journal*, vol. 13, no. 10, pp. 3568–3574, Oct. 2013.
- [2] T. Chen, Y. Shen, Q. Ling, and G. Giannakis, "Online learning for thing-adaptive fog computing in IoT," in *ASILOMAR*, Pacific Grove, USA, Oct. 2017.
- [3] Q. Wu, G. Ding, and Y. Xu, "Cognitive internet of things: A new paradigm beyond connection," *IEEE Internet of Things Journal*, vol. 1, no. 2, pp. 129–143, Apr. 2014.
- [4] S. Yu, M. Liu, W. Dou, X. Liu, and S. Zhou, "Networking for Big Data: A survey," *IEEE Communications Surveys and Tutorials*, vol. 19, no. 1, pp. 531–549, 2017.
- [5] A. Carroll and G. Heiser, "An analysis of power consumption in a smartphone," in *Proceedings of the 2010 USENIX Conference on USENIX Annual Technical Conference*. Berkeley, CA, USA: USENIX Association, Jun. 2010, pp. 21–21.
- [6] K. Georgiou, S. Xavier-de-Souza, and K. Eder, "The IoT energy challenge: A software perspective," *IEEE Embedded Systems Letters*, pp. 1–4, Aug. 2017.

- [7] S. Yu, W. Zhou, S. Guo, and M. Guo, "A feasible IP traceback framework through dynamic deterministic packet marking," *IEEE Transactions on Computers*, vol. 65, no. 5, pp. 1418–1427, May. 2016.
- [8] H. Zhang, Y. Qiu, X. Chu, K. Long, and V. C.M.Leung, "Fog radio access networks: Mobility management, interference mitigation, and resource optimization," *IEEE Wireless Communications*, vol. 24, no. 6, pp. 120–127, Dec. 2017.
- [9] X. Lu, D. Niyato, P. Wang, D. I. Kim, and Z. Han, "Wireless charger networking for mobile devices: Fundamentals, standards, and applications," *IEEE Wireless Communications*, vol. 22, no. 2, pp. 126–135, Apr. 2015.
- [10] A. Costanzo, M. Dionigi, D. Masotti, M. Mongiardo, G. Monti, L. Tarricone, and R. Sorrentino, "Electromagnetic energy harvesting and wireless power transmission: A unified approach," *Proceedings of the IEEE*, vol. 102, no. 11, pp. 1692–1711, 2014.
- [11] S. Valtchev, E. Baikova, and L. Jorge, "Electromagnetic field as the wireless transporter of energy," *Facta universitatis - series: Electronics and Energetics*, vol. 25, no. 3, pp. 171–181, Dec. 2012.
- [12] S. Assaworarith, X. Yu, and S. Fan, "Robust wireless power transfer using a nonlinear parity-time-symmetric circuit," *Nature*, vol. 546, no. 7658, p. 387, Jun. 2017.
- [13] B. Cannon and J. Hoburg, "Magnetic resonant coupling as a potential means for wireless power transfer to multiple small receivers," *IEEE Transactions on Power Electronics*, vol. 24, no. 7, pp. 1819–1825, Jul. 2009.
- [14] Z. Popovic, "Cut the cord: Low-power far-field wireless powering," *IEEE Microwave Magazine*, vol. 14, no. 2, pp. 55–62, Apr. 2013.
- [15] J. Fakidis, S. Videv, H. Helmers, and H. Haas, "0.5-Gb/s OFDM-based laser data and power transfer using a GaAs photovoltaic cell," *IEEE Photonics Technology Letters*, pp. 1–1, Mar. 2018.
- [16] A. Sahai and D. Graham, "Optical wireless power transmission at long wavelengths," in *2011 International Conference on Space Optical Systems and Applications (ICSOS)*, Santa Monica, CA, USA, May 2011, pp. 164–170.
- [17] Q. Liu, J. Wu, P. Xia, S. Zhao, W. Chen, Y. Yang, and L. Hanzo, "Charging unplugged: Will distributed laser charging for mobile wireless power transfer work?" *IEEE Vehicular Technology Magazine*, vol. 11, no. 4, pp. 36–45, Dec. 2016.
- [18] Q. Zhang, X. Shi, Q. Liu, J. Wu, P. Xia, and Y. Liao, "Adaptive distributed laser charging for efficient wireless power transfer," in *2017 IEEE 86th Vehicular Technology Conference (VTC2017-Fall)*, Toronto, ON, Canada, Sep. 2017, pp. 1–5.
- [19] W. Koechner, *Solid-State Laser Engineering*, 6th ed. Springer, 2006.
- [20] S. Cao, S. Tu, Y. Huang, H. Fan, J. Li, H. Xia, and G. Ren, "The analysis in the resonator diffraction losses of the laser modes," *Laser Technology*, vol. 42, no. 3, pp. 400–403, Sep. 2018.
- [21] M. S. Aziz, S. Ahmad, and I. Husnaini, "Simulation and experimental investigation of the characteristics of a PV-harvester under different conditions," in *International Conference on Energy Systems and Policies*, Nov. 2014, pp. 1–8.
- [22] A. G. Martin, E. Keith, H. Yoshihiro, W. Wilhelm, and D. D. Ewan, "Solar cell efficiency tables (Version 45)," *Progress in photovoltaics: research and applications*, vol. 23, no. 1, pp. 1–9, 2015.
- [23] L. Summerer and O. Purcell, "Concepts for wireless energy transmission via laser," in *International Conference on Space Optical Systems and Applications*, 2008.
- [24] H. Kogelnik, "Imaging of optical modes - resonators with internal lenses," *The Bell System Technical Journal*, vol. 44, no. 3, pp. 455–494, Mar. 1965.
- [25] H. Kogelnik and T. Li, "Laser Beams and Resonators," *Applied Optics*, vol. 5, no. 10, pp. 1550–1567, Oct. 1966.
- [26] V. Magni, "Resonators for solid-state lasers with large-volume fundamental mode and high alignment stability," *Applied Optics*, vol. 25, no. 1, pp. 107–117, Jan. 1986.
- [27] B. Zhou, Y. Gao, and J. Chen, *Laser Principle*, 6th ed. Beijing: The National Defense Press, 2004.
- [28] G. Wei and B. Zhu, *Laser Beam Optics*, 1st ed. Beijing: Beijing Industry Collage Press, 1988.